Florida International University
FIU Digital Commons

Electrical and Computer Engineering Faculty Publications

College of Engineering and Computing

Physics considerations in targeted anticancer drug delivery by magnetoelectric nanoparticles

Emmanuel Stimphil
Department of Electrical and Computer Engineering, Florida International University, estimphi@fiu.edu

Abhignyan Nagesetti
Department of Electrical and Computer Engineering, Florida International University, anageset@fiu.edu

Rakesh Guduru
Herbert Wertheim College of Medicine and College of Engineering, Florida International University, rguduru@fiu.edu

Tiffanie Stewart
Herbert Werthiem College of Medecine, Florida International University, tsstewar@fiu.edu

Alexandra Rodzinski
Herbert Wertheim College of Medicine, Florida International University, arodzins@fiu.edu

See next page for additional authors

Recommended Citation

Authors

Emmanuel Stimphil, Abhignyan Nagesetti, Rakesh Guduru, Tiffanie Stewart, Alexandra Rodzinski, Piang Liang, and Sakhrat Khizroev

APPLIED PHYSICS REVIEWS—FOCUSED REVIEW

Physics considerations in targeted anticancer drug delivery by magnetoelectric nanoparticles

Emmanuel Stimphil,[1] Abhignyan Nagesetti,[1] Rakesh Guduru,[1] Tiffanie Stewart,[2] Alexandra Rodzinski,[2] Ping Liang,[3] and Sakhrat Khizroev[1,2,a]

[1]*Department of Electrical and Computer Engineering, Florida International University, Miami, Florida 33174, USA*
[2]*Department of Cellular Biology and Pharmacology, Herbert Wertheim College of Medicine, Florida International University, Miami, Florida 33199, USA*
[3]*Electrical and Computer Engineering, University of California, Riverside, California 92521, USA*

In regard to cancer therapy, magnetoelectric nanoparticles (MENs) have proven to be in a class of its own when compared to any other nanoparticle type. Like conventional magnetic nanoparticles, they can be used for externally controlled drug delivery via application of a magnetic field gradient and image-guided delivery. However, unlike conventional nanoparticles, due to the presence of a non-zero magnetoelectric effect, MENs provide a unique mix of important properties to address key challenges in modern cancer therapy: (i) a targeting mechanism driven by a physical force rather than antibody matching, (ii) a high-specificity delivery to enhance the cellular uptake of therapeutic drugs across the cancer cell membranes only, while sparing normal cells, (iii) an externally controlled mechanism to release drugs on demand, and (iv) a capability for image guided precision medicine. These properties separate MEN-based targeted delivery from traditional biotechnology approaches and lay a foundation for the complementary approach of technobiology. The biotechnology approach stems from the underlying biology and exploits bioinformatics to find the right therapy. In contrast, the technobiology approach is geared towards using the physics of molecular-level interactions between cells and nanoparticles to treat cancer at the most fundamental level and thus can be extended to all the cancers. This paper gives an overview of the current state of the art and presents an *ab initio* model to describe the underlying mechanisms of cancer treatment with MENs from the perspective of basic physics. *© 2017 Author(s). All article content, except where otherwise noted, is licensed under a Creative Commons Attribution (CC BY) license (http://creativecommons.org/licenses/by/4.0/).* [http://dx.doi.org/10.1063/1.4978642]

TABLE OF CONTENTS

I. INTRODUCTION

Achieving adequately high specificity to target cancer cells while sparing normal cells remains one of the greatest challenges in cancer therapy to date.[1–3] Ongoing research has attempted to address this fundamental challenge by using nanoparticles as targeted delivery vehicles. Due to their small sizes and unique shapes, nanoparticles can help steer a therapeutic load to specific targets and meet a wide range of requirements for overcoming numerous biological barriers.[4–10] There are endless types of nanoparticle delivery systems, both passive and active, constantly being developed. Passive systems mostly rely on exploiting the enhanced permeability and retention (EPR) effect, which exists due to the high leakiness

[a]Author to whom correspondence should be addressed. Electronic mail: khizroev@fiu.edu. Telephone: 1-305-348-3724.

of tumor blood vessels and the lack of a lymphatic system for drainage.[11–14] The delivery specificity can be further improved by adding an active delivery mechanism, for example, through conjugating nanoparticles with monoclonal antibodies (mAbs) tailored to recognize over-expressed tumor-specific biomarkers.[15–21] In addition, nanoparticles must be able not only to provide high-specificity targeted delivery but also to ensure that the therapeutic load is not prematurely released in the plasma or interstitial space before it reaches the intended target.[22–25] Therefore, nanoparticles have been further functionalized to control drug release by externally applied temperature,[26,27] ultrasound,[28,29] intracellular pH level,[30] intracellular enzymes,[31] or magnetic fields.[32–35] Nevertheless, all these approaches still have inadequately low efficacy.

In parallel, there has been a focus on using the phenomenon of electroporation for enabling a high-efficacy high-specificity cellular uptake of a drug.[36–43] In this case, an electric field above a cell-specific threshold causes a dielectric breakdown of the cell membrane.[44] This breakdown field is different for cancer and normal cells of the same type. For example, application of an electric field on the order of 1 kV/cm can create sufficiently large pores allowing for an enhanced cellular uptake of molecules by cancer cells while it takes a factor of two or five higher field to achieve this effect in the normal cells. Although very promising, the electroporation involves relatively high electric fields at a relatively large scale and thus comes with a collateral damage.

Based on an analysis of recent studies,[45–49] combined with a new study on using liquid-environment atomic force microscopy (AFM) to study the interaction between nanoparticles and the cellular membranes, this paper presents a basic physics model to help understand how a class of multiferroic nanoparticles known as magnetoelectric nanoparticles (MENs) could address the above challenges.[50–53] Indeed, MENs provide (a) a targeting mechanism driven by a physical force rather than antibody matching, (b) a delivery mechanism that enhances cellular uptake of a therapeutic load across the cancer cell membranes only, without affecting normal cells, (c) an externally controlled mechanism that releases the load on demand, last but not least (d) due to the presence of a magnetic moment, they can be used for image-guided therapy. With the above said, MENs present a novel platform to treat cancer not from the perspective of bioinformatics but rather from the perspective of the molecular-level physics of the interaction between nanoparticles and cellular microenvironment. Such an approach, hereinafter referred to as technobiology, is complementary to the traditional biotechnology approach.

II. UNDERLYING PHYSICS

A. Difference between MENs and magnetic nanoparticles (MNPs)

MENs must not be confused with traditional magnetic nanoparticles (MNPs), e.g., superparamagnetic iron oxide nanoparticles (SPIONs)[54–57] or other superparamagnetic and non-superparamagnetic ferromagnetic or ferrimagnetic nanostructures used for targeted delivery or magnetic imaging.[58–61] Like MNPs, MENs have a non-zero magnetic moment and therefore can be transported via application of an external d.c. magnetic field with a non-zero spatial gradient. Also, the negative feedback loop required for image-guided navigation can be closed through existing magnetic imaging techniques such as magnetic resonance imaging (MRI) or magnetic particle imaging (MPI).[62–64] However, unlike MNPs, MENs offer a novel functionality—an energy-efficient control of intrinsic electric fields in close proximity to the nanoparticles via application of external d.c. and a.c. magnetic fields. Due to the magnetoelectric effect (ME) effect, MENs allow an external control of the electric fields that underlie the intrinsic molecular interactions between specific cells and the drug-loaded nanoparticles as well as the interaction between MENs and the loaded drug. An immediate consequence of this capability is the freedom to engineer an adequately strong bond between the nanoparticles and the drug to avoid an undesired release of the therapeutic load before it reaches the target; only when an a.c. magnetic field is applied, this strong bond is "turned off" on demand. This mechanism of using an a.c. field to controllably break the bond between MENs and the load has been previously described with regard to the topic of delivery of antiretroviral therapy across the blood-brain barrier (BBB) to treat HIV-1 virus hidden deep in the brain.[65] In addition, due to the ME effect, using MENs opens a pathway to exploit intrinsic electric properties of the cell membrane at the nanoscale for enabling targeted high-specificity delivery without relying on any bioactive mechanism. The cell membrane, consisting of numerous ion channels, is an electrically polarizable medium, and its electric charge strongly depends on the cellular microenvironment, e.g., its pH level. As a result, cellular properties can be significantly and differently (for normal and cancer cells) affected by local electric fields.[66,67] This difference is the basis for using electroporation for inducing a high-specificity drug uptake by cancer cells. According to the conventional approach to an electroporation-based cancer treatment, a relatively large electric field, on the order of 1000 V/cm, is applied at the macroscale, which inevitably results in undesired side effects. With MENs, this property of electroporation can be scaled down to the nanoscale. As a result, the MEN-induced electroporation, hereinafter referred to as nanoelectroporation, would result in significantly reduced side effects because the relatively high field is limited to the nanoscale region in proximity to each nanoparticle. In addition, the specificity factor (SF), defined as the ratio of the average number of nanoparticles penetrated into a cancer cell versus the average number of nanoparticles penetrated into an adjacent normal cell under equivalent conditions, can be significantly increased in the case of the nanoelectroporation, as discussed below in more detail. Due to this nanoelectroporation ability, MENs not only further improve the specificity of the EPR-based delivery but also add another targeting mechanism to enable passive delivery at the intracellular level and thus pave a way to treatment of both primary and secondary tumors at different cancer progression levels. Last but not least, because of the fundamental nature of this externally controlled approach, MENs can be used to treat all kinds of cancers including fast-progressing brain tumors and other

solid and liquid tumors. Brachytherapy would be one example of a current approach which could be completely replaced by MENs. Brachytherapy uses a sealed radioactive pellet, e.g., made of iridium, placed close to a tumor site through catheters.[72] When activated, the pellet emits radiation which kills both cancer and normal cells a few millimetres away. Using field-activated MENs instead of the strongly radioactive pellet can significantly improve the specificity of the treatment and thus reduce or eliminate side effects.

B. Synthesis and characterization of MENs

MENs can be synthesized according to standard chemical procedures described in previous studies. One of the most popular room-temperature configurations is the core-shell nanostructure made of a magnetostrictive core, e.g., $CoFe_2O_4$, and a piezoelectric shell, e.g., $BaTiO_3$.[68–71] By default, in this paper, the average size of MENs is approximately 30 nm and the average size of the core is approximately 10 nm. X-Ray diffraction (XRD) measurements have confirmed the cubic and tetragonal crystal structures of the core and shell, respectively. Depending on a specific application, whether it is for a drug delivery, a neural stimulation, or 3D navigation and/or imaging, MENs can be further coated with thin functionalization layers serving as linkers to the therapeutic load or to enable hydrophilic or hydrophobic surface suitable for the microenvironment of interest. The ME coefficient, α, for these nanostructures is known to be in a range from 10 to over 100 mV cm^{-1} Oe^{-1}, depending on the phase compositions and the quality of the interface between the core and the shell. The saturation magnetization of these particular MENs is on the order of 10 emu/g, which is an order of magnitude smaller than that for high-moment iron oxide nanoparticles. Considering the core is made of a relatively high anisotropy structure, these MENs are not superparamagnetic and have a room temperature coercivity on the order of 100 Oe. On a final note, it is worth noting that in general MENs are not limited to this particular composition. There are many other compositions which display a non-zero ME effect. Furthermore, it is likely that in the future MENs will be made of biodegradable organic materials; for example, carbon based nanostructures have already been shown to display a non-zero ME effect.[73]

C. Targeting by MENs

In general, there are two fundamentally different approaches to targeting with MENs, using local and systemic administration of nanoparticles, respectively. For the local administration, MENs could be either directly injected into a tumor site or navigated to the target site via application of localized magnetic fields after the nanoparticles are administrated in the vasculature. For example, it has been shown that using MRI-guided navigation with a pulsed sequence of field gradients, magnetic nanoparticles could be localized at any point in a 3D space with a spatial precision of less than 0.1 mm.[74] For the systemic administration, MENs could be administrated intravenously. In either case, the delivery and uptake specificity could be further significantly improved due to the following physics.

Unlike purely active delivery approaches, e.g., using mAbs, T-cells (CAR T-Cell), or cancer vaccines, MENs offer a passive delivery mechanism, which is complementary to the well-known EPR effect.[75] The EPR effect ensures delivery of drug-loaded nanoparticles into relatively large tumor aggregates but not in relatively small aggregates made of one or few cancer cells. In contrast, due to a different underlying physics, MENs-driven targeting works equally well with cell aggregates and individual cells. Because MENs generate their own electric fields, which in turn can be controlled by external magnetic fields, they can specifically electroporate cancer cells without affecting surrounding normal cells, as described below in more detail. In this case, the localization range of the nanoparticle-generated electric field is defined by the nanoparticle's average size, which is approximately 30 nm. In turn, this localization range is orders of magnitude smaller than the characteristic cell size, which is on the order of a few microns. Therefore, MENs could be used to target primary and metastasized cancer cells even at a very early stage of cancer progression. Last but not least, because of the existence of an externally controlled surface charge, MENs bring another dimension to targeted delivery; not only can they increase the specificity factor but also can provide new functions of externally controlled cancer cell penetration and drug release via application of external magnetic fields. In a trivial approximation, the electric field generated by a MEN at a point on the cell membrane consists of two terms:

$$E = k\frac{3(p \cdot \hat{r})\hat{r} - p}{r^3} + \frac{kQ}{r^2}\hat{r}, \qquad (1)$$

where k is the Coulomb constant, Q and p are the MEN's electric charge and dipole moment, respectively, and r is the distance between the nanoparticle and the observation point on the membrane. The first term is determined by the magnetic-field dependent electric dipole moment due to the ME effect, $p = \alpha H$, where α is the ME coefficient and H is the external magnetic field. The second term is determined by the surface electric charge which is formed according to the colloidal chemistry when MENs are placed in a solution, e.g., the blood or the lymph. In this case, a double charged layer is formed around the nanoparticle's surface because of the interplay of chemical and electrical forces. The surface charge can be determined by measuring Zeta potential. Furthermore, previously it has been shown that this surface charge can be further increased with an external magnetic field increase; in other words, the field dependence of the surface charge also depends on the ME effect. It can be noted that the surface charge term has a more significant effect because it drops with a distance substantially slower ($\sim 1/r^2$) compared to the dipole charge term ($\sim 1/r^3$).

Because both MENs and the cell membranes have the same charge polarity, MENs can easily go through a capillary without being engulfed by the surrounding cells. However, when MENs are in close proximity to the cell membranes (within a distance on the order of a micron), their electric field (on the order of 0.1 V/μm, as shown below mostly due to the charge) is sufficiently strong to induce a

(a)   (b)

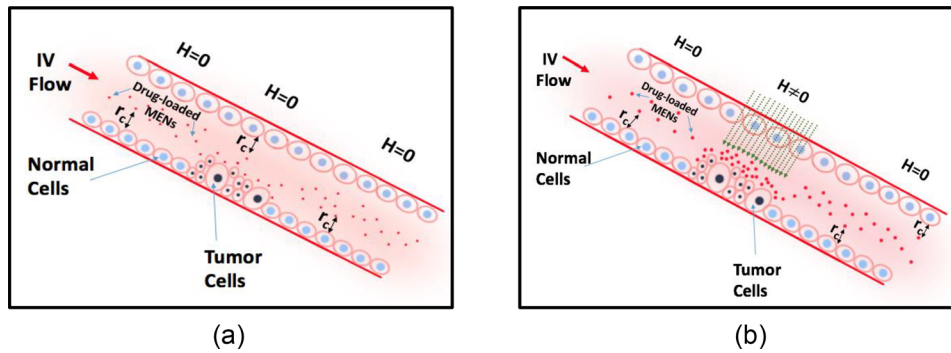FIG. 1. Illustration of the dependence of the cutoff distance, rc, on application of an external d.c. magnetic field, H. (a) The nanoparticles within this distance from the membrane surface target the cancer cells due to the high-specificity nanoelectroporation effect. (b) The distance is increased with an increase in the magnetic field.

local dielectric breakdown in the cancer cells but not too strong ($\lesssim 1.5$ V/μm) where it may cause this effect in the normal cells. This dielectric breakdown is reflected in a local change of the lipid bilayer of the cellular membrane. Such a field-dependent local change leads to cellular uptake of the drug-loaded nanoparticles through the membrane surface. Indeed, it is known that the conductivity of the intermediate cancer cell membrane is by three orders of magnitude larger than that of the normal cell membrane.[77] The high-conductivity membrane induces a local attraction force between MENs and the cancer cell due to the electrostatic "mirror" effect. Here, it is worth noting that this nanoelectroporation effect could be further increased through application of a pulsed magnetic field sequence. In this case, the intermediate high-conductivity breakdown state effectively lasts longer and thus the efficacy of this treatment is significantly increased. That is the reason why the a.c. field application might be more effective compared to the d.c. field application. However, to simplify the explanation, the following description is focused on the d.c. case. In a first order approximation, there are two distinct states of the membrane. In its normal state, the membrane is non-conducting. In this case, the negatively charged MENs are pushed away from the negatively charged membrane surface. On the contrary, during the intermediate nanoelectroporation process, the membrane surface of the cancer cells is conducting and thus MENs are attracted to the cancer cells. According to the "mirror image" model, the attraction force could be estimated with this expression,

$$F_{mirror} = kQ^2/4r^2, \qquad (2)$$

where the factor $^1/_4$ is due to the fact that the effective distance between the real and image charges is 2r, while r is the distance between the nanoparticle and the membrane surface. Furthermore, as previously shown, the effective surface charge and thus this attraction force can be further increased with an increase in the externally applied magnetic field. This magnetic field dependence of the charge can be found through an experimental measurement of Zeta potential, V(H), in a phosphate buffer solution (PBS) with a pH level similar to that in the blood, Q = V(H)d/k. Now, it is possible to estimate the cut-off distance between the nanoparticle and the membrane surface, r_C, below which the electric field would be above the nanoelectroporation threshold on the order of 0.1 V/μm for the cancer cells: $r_C = 0.5(kQ/E)^{1/2}$. For example, it has been shown that application of a magnetic field on the order of 300 Oe could increase the cut-off distance by a factor of

two. Such an increase would significantly increase the number of the nanoparticles capable of triggering local nanoelectroporation and consequently would significantly increase the specificity factor of targeted delivery. This concept of MEN-based targeting is illustrated in Figure 1. It could be noted that this overly simplified theory does not take into account the laminar flow in the circulation.

D. Drug release on demand

After the drug-loaded MENs enter the cancer cells, the drug can be released off the nanoparticles on demand via application of an a.c. external magnetic field. In this case, as previously shown, even a relatively small magnitude a.c. field ($\lesssim 50$ Oe) in the near-d.c. frequency ranging from 10 to over 100 Hz is sufficiently strong to release substantial amount of the drug into the cancer cells. It has been hypothesised that application of an a.c. field "shakes" the drug off the nanoparticles by significantly weakening the electric-field bond which holds the two together, as illustrated in Fig. 2. According to the trivial model, the electric dipole moment induced by an external magnetic field due to the ME effect is $\Delta P = \alpha H$; therefore, the displaced surface charge density on the diametrically opposite side of the nanoparticle would be $\sigma_{ME} \sim \pm \alpha H$. In other words, the magnetically triggered electric dipole moment breaks the symmetry of ionic bonds around the nanoparticle. To a zeroth approximation, when the displaced surface charge is comparable to the charge involved in an original bond, $\sigma_{ME} \sim Q_{ionic}/\pi d^2$, the bond can be broken. Then, the threshold magnetic field amplitude to break a bond can be evaluated according to this simple expression:

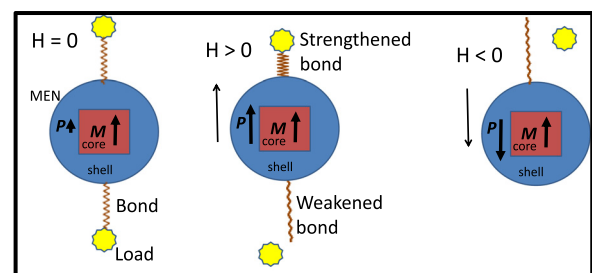$$H_{th} \sim Q_{ionic}/\pi d^2 \alpha, \qquad (3)$$

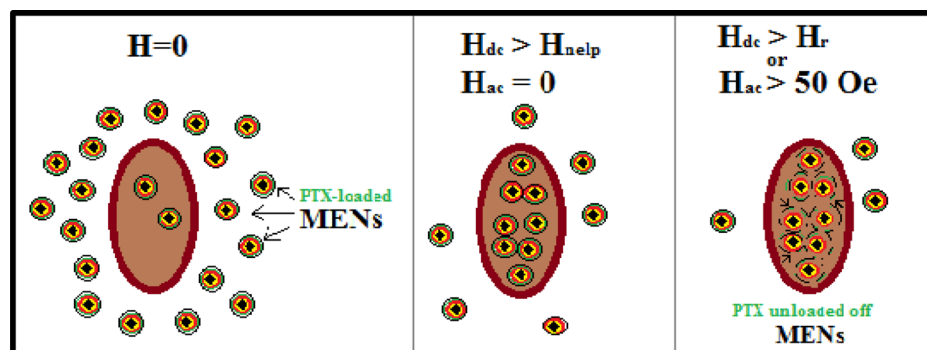FIG. 2. Illustration of the drug release mechanism via application of an a.c. magnetic field.

FIG. 3. Illustration of a field-controlled targeted drug (PTX) delivery and release by MENs.

where d is the diameter of the nanoparticle, α is the ME coefficient, and Q_{ionic} is the displaced charge in the ionic bond. Application of an a.c. field would break the bonds in all the orientations around the nanoparticle.

Here, it is worth reminding that it is imperative to release the drug off MENs to increase the drug bioactivity only after the drug-loaded MENs penetrate the cancer cells.[76] In other words, MENs enable a drug retention control via application of external magnetic fields; the initial step of high-specificity cellular penetration and the final step of drug release off MENs are triggered via application of d.c. and a.c. fields, respectively.

In summary, the above described three-step field-controlled process for targeted drug delivery and release, respectively, is illustrated in Fig. 3.

III. SUPPORTING EXPERIMENTS

A. Confocal microscopy study of high-specificity cellular penetration

The purpose of the first described *in vitro* experiment was to show how an external d.c. magnetic could be used to induce a penetration of drug-loaded MENs into cancer cells. A popular mitotic inhibitor paclitaxel (PTX) was used as the therapeutic load. In the described microscopy experiments, the PTX's fluorescent version known as Flutax-2 was imaged at 488 nm (green color). A multidrug resistant cancer cell line MES-SA/DX5 was used to test the field-induced penetration. For comparison, similar images were taken for two other cases with cells incubated under equivalent conditions without any drug and just with the drug, respectively. Microscopy images of the

two control cases and the cells incubated with MENs without and with exposure to a d.c. field of 30 Oe for approximately 12 h are shown in Figs. 4(a)–4(d), respectively. The optically measured percentages of the drug uptake per mg of protein in the four cases were 0, less than 0.3%, less than 0.2%, and more than 6%, respectively. According to the procedures of the experiment, the green light could be seen only from the drug coming from inside the cells, because all the extracellular material was washed away. The experiment clearly showed a strong field dependence of the cellular uptake of the drug-loaded MENs. Indeed, the uptake of the drug increased from less than 0.2% to over 6%, i.e., by a factor of 30, after application of a relatively small d.c. field of 30 Oe.

Another experiment was conducted to demonstrate a high-specificity cellular uptake with MEN-based delivery on ovarian cancer and normal cell lines SKOV-3 and HOMEC, respectively. The optically measured drug uptake depending on the applied d.c. magnetic field for cancer and normal cells is shown in Fig. 5. Indeed, it could be observed that there was a significant field range, from ~50 Oe to ~500 Oe, when visibly large amount of the drug penetrated the cancer cells while barely any drug penetrated the normal cells. As mentioned earlier, the effect of nanoelectroporation could be further increased via application of a periodic sequence of magnetic field pulses to effectively prolong the membrane's intermediate dielectric breakdown state which leads to the nanoparticles' cellular uptake. Application of an a.c. magnetic field partially mimics this pulsed sequence effect.[53] Indeed, this a.c. field dependence was demonstrated in the same experimental study.

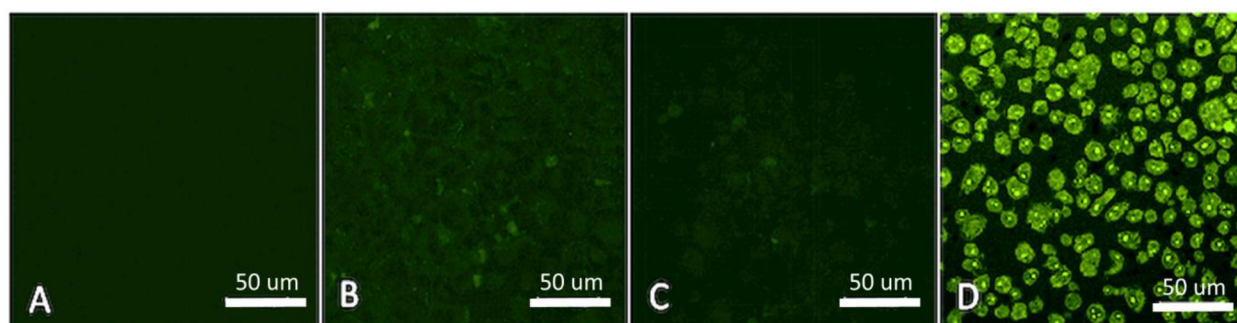Another experiment which demonstrated the field-dependent cellular penetration of MENs was conducted with

FIG. 4. Confocal microscopy imaging of the uptake of Flutax-2 by cell line MES-SA/DX5 for four different drug-delivery-system combinations: (a) no drug, (b) free Flutax-2 (drug uptake per mg of protein: <0.3%), (c) MENs loaded with Flutax-2 with no field (<0.2%), and (d) MENs loaded with Flutax-2 in a 30 Oe d.c. field (>6%). The scale bar is approximately 50 um.
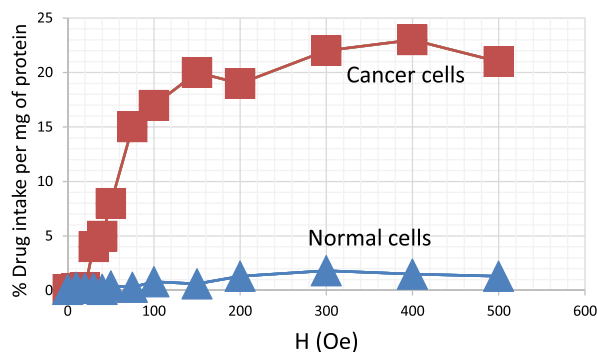
FIG. 5. Optically measured (with a fluorometer) field dependence of the drug uptake per mg of protein for cancer and normal cell lines SKOV-3 and HOMEC, respectively.

atomic force microscopy (AFM) and magnetic force microscopy (MFM) imaging of cell lysates. This experiment directly confirmed the presence of MENs inside cancer cells only after application of a 100-Oe d.c. field.

B. Drug release off MENs via application of an a.c. field

The purpose of the following experiments was to prove that the therapeutic load could be released off MENs via application of an a.c. magnetic field. Consequently, the function of the drug release could be physically separated from the function of high-specificity targeting, in turn, achieved via application of a d.c. field.

In one experiment, the amount of the released drug (paclitaxel) was measured spectrophotometrically at its maximum absorption wavelength of approximately 230 nm. It is known that the bioactivity of the drug significantly increases after the release due to the increased "free" surface area. The dependence of the released drug on the strength and frequency of the a.c. field ranging from 12 to 66 Oe and 0 to 1000 Hz, respectively, for different application times ranging from 1 min to 2 h, is shown in a chart in Fig. 6.

Other experiments to confirm the drug release via application of an a.c. field were based on Fourier-transform infrared (FTIR) spectroscopy and X-ray diffraction (XRD) measurements.
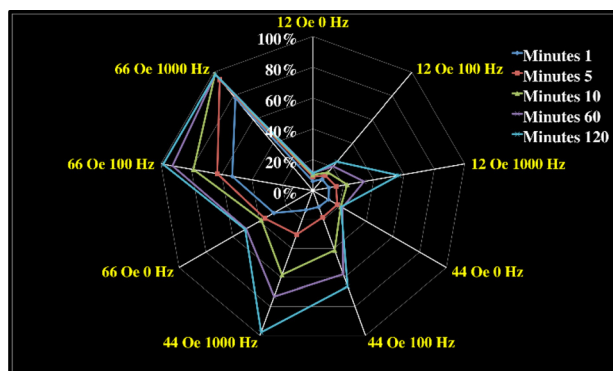

FIG. 6. The dependence of the release of the drug, paclitaxel, on the a.c. field strength and frequency for five different application times: 1, 5, 10, 60, and 120 min. The data were measured spectrophotometrically as the absorbance at 230 nm wavelength.

C. Liquid-environment atomic force microscopy study of the nanoparticle-cell interaction

A liquid environment atomic force microscopy (AFM) study was conducted with the goal to directly measure the surface of cancer and normal cells under different experimental conditions. In the following experiment, glioblastoma (U87-MG) and endothelial cells were used as the cancer and normal cells, respectively. Glioblastomas represent the most frequent primary brain tumors while endothelial cells are characteristic normal brain cells. It was already demonstrated that drug-loaded MENs could be navigated across the blood-brain barrier (BBB) via application of a sufficiently strong d.c. magnetic field gradient (on the order of 1000 Oe/cm) with the subsequent controlled release of the drug after the nanoparticles are placed deep in the brain.[65] Typical AFM images of endothelial and glioblastoma cells are shown in Figs. 7(a) and 7(b), respectively. It can be noted that the normal cells have a more continuous surface morphology compared to the cancer cells with clearly visible striations with a characteristic size on the order of 100 nm.

Another AFM experiment was conducted to understand how MENs penetrated the cancer cells. MENs were added into media with glioblastoma cells through a special Multimode liquid environment microprobe container. Here, it is worth noting that usually when nanoparticles or other nanoscale foreign reagents get attached to the membrane surface, they quite rapidly (within seconds) move across the membrane and penetrate the cell. The exact origin of this process still remains an open question; it might
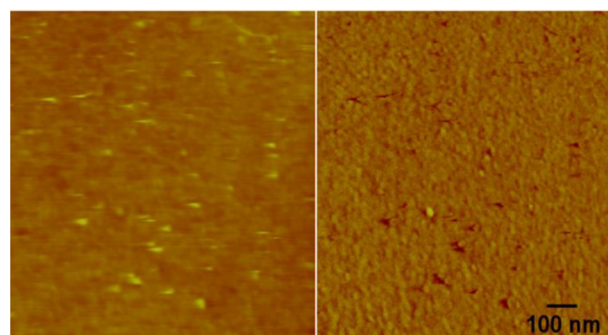
(a)
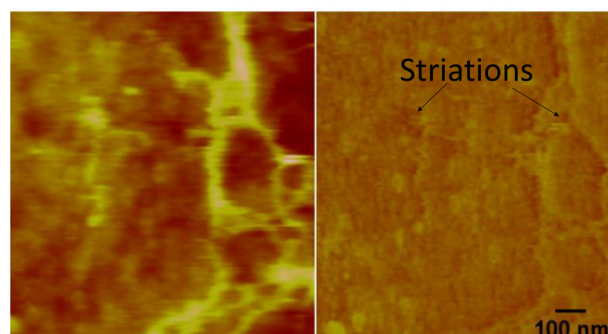
(b)

FIG. 7. AFM image pair (z height and phase (right)) for (a) endothelial and (b) glioblastoma cells.

be defined either by a chain signalling between biomolecules within the cell or by some electric field effects in the membrane and the cellular plasma or a combination of these two effects. It is not trivial to use AFM to observe the fast dynamic of the nanoparticle-cell interaction. To slow down the cellular uptake of the nanoparticles, this experiment was conducted at a relatively high concentration of MENs to ensure the cells are saturated and as a result the nanoparticles become visible on the membrane surface. An important observation of this experiment was the fact that the nanoparticles preferred to penetrate the cancer cell through the striations in the cellular membrane, as shown in Fig. 8.

Last but not least, it could be mentioned that MENs operate at relatively low fields and frequencies and thus do not cause significant heating effects, as was confirmed through infrared measurements of the cell surface at different concentrations of MENs under different field exposures.

IV. CONCLUSION

The discussed experiments have demonstrated that MENs could be used for externally controlled targeted drug delivery and release. Furthermore, these two important functions, i.e., delivery and release, could be physically separated via application of d.c. and a.c. external magnetic fields, respectively, as indicated by the hypothesised theory and confirmed by a number of independent experiments. For example, confocal microscopy studies have directly confirmed that the penetration of MENs into cancer cells occurs only after the application of a d.c. magnetic field on the order 100 Oe, while numerous spectrophotometry measurements have shown that the drug is released off the nanoparticles only after the application of an a.c. magnetic field with a strength on the order of 50 Oe and a near-d.c. frequency of 100 Hz. As for the high-specificity delivery, one of the most important characteristics of MENs is their ability to deliver drugs specifically into the cancer cells without affecting the surrounding normal cells. The penetration fields due to the nanoelectroporation, i.e., the mechanism according to which the delivery takes place, are different for the two cell forms, i.e., cancer and normal cells, respectively, because their membranes have different surface morphologies and charge configurations, as shown through transport measurements

and AFM studies. As a result, it takes a significantly higher field to break the dielectric barrier of the normal cell membranes compared to that of the cancer cells. As mentioned above, it is well known that even at the macroscale, the cancer cells have a smaller threshold field for the electroporation compared to their normal counterparts; the difference is a factor of two to five depending on the cancer type. The discussed experiments with MENs have shown that at the nanoscale the difference becomes even more significant. For example, for the ovarian and normal cancer cell lines, SKOV-3 and HOMEC, respectively, it takes less than 100 Oe and significantly more than 1000 Oe, respectively, to induce the nanoelectroporation via the ME effect. That is the reason why we refer to the electroporation (by MENs) at the nanoscale as the nanoelectroporation. The nanoelectroporation seems to have a significantly higher specificity factor compared to the traditional electroporation effect which takes place at the macroscale. The AFM imaging of equivalent glioblastoma cancer and normal endothelial cells has shown very different surface topographies for the two cell types; the normal cells are more continuous compared to the cancer cells which in turn have visible striations of the characteristic size on the order of 100 nm. The AFM images have also shown that 30-nm MENs tend to accumulate in these striations and thus penetrate the cell through these striations. The fact that the nanoparticles penetrate the cancer cells through the small striations in the membrane might explain why the ratio between the nanoelectroporation threshold fields between cancer and normal cells is more significant ($\gtrsim$10) compared to that for the traditional electroporation at the macroscale ($\sim$2–5). It is worth noting that due to the intrinsic nature of the ME coupling in the multiferroic nanostructures, the magnetic field strength on the order of 100 Oe, required for enabling the high-specificity delivery and release functions, is substantially below any harmful limits as per US Food and Drug Administration (FDA) regulations.[78] Eventually, because of the fundamental nature of this approach, it can be applied to any cancer type. Last but not least, it can be mentioned that most current studies have been performed with MENs of the same coreshell composition, i.e., $CoFe_2O_4$–$BaTiO_3$. These experiments have been vital to demonstrate the feasibility of the MEN-based cancer treatment approaches. In the future, other compositions can be explored, e.g., ones made of biodegradable organic materials.
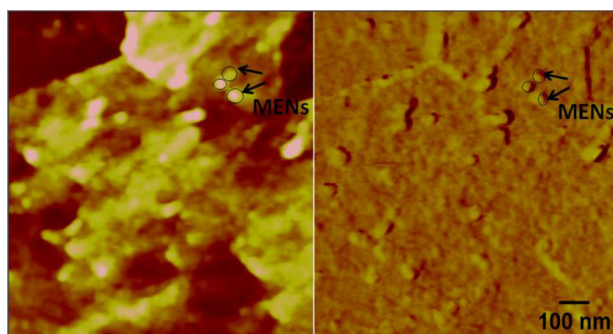
V. MATERIALS AND PROCEDURES

A. Chemical synthesis of MENs

$CoFe_2O_4$-$BaTiO_3$ core shell MENs were prepared according to a polyvinylpyrrolidone assisted hydrothermal method. First, 0.058 g of Cobalt Nitrate Hexahydrate ($Co(NO_3)_2 \cdot 6H_2O$) and 0.16 g of Ferric Nitrate Nonahydrate ($Fe(NO_3)_3 \cdot 9H_2O$) were dissolved by stirring in 15 ml of distilled water. Polyvinylpyrrolidone (PVP), 0.2 g, was dissolved in 5 ml of aqueous solution containing 0.9 g of sodium borohydride. The PVP-sodium borohydride solution was added dropwise to the above solution and the mixture was stirred at 120 °C until the liquid phase evaporated.

FIG. 8. AFM image pair (z height and phase (right)) for glioblastoma cells with MENs found in striations on the surface membrane. The observed nanoparticles are approximately 30-nm in diameter.

$CoFe_2O_4$ particles were recovered, dispersed in distilled water through sonication, and washed 3 times using magnetic separation. Purified $CoFe_2O_4$ cores were dried at 120 °C for 24 h and stored at room temperature until further use. The Barium Titanate ($BaTiO_3$) shell was prepared using the citrate gel method. Briefly, $CoFe_2O_4$ cores were dispersed in distilled water through sonication. Barium Carbonate ($BaCO_3$), 174 mg, was dissolved in 60 ml deionized water containing 1 g of citric acid. This solution was mixed with a 150 ml ethanolic solution of titanium (IV) isopropoxide (284 μl) and 6 g citric acid. The BaTi precursor solution was added to the cores and sonicated at room temperature for 1 h. The translucent yellow liquid was stirred at 70 °C until the liquid phase evaporated completely. Finally, the gel was calcined at various temperatures ranging from 500 to 800 °C (CMF-1100) for 5 h and cooled naturally to room temperature. The gelation temperature and the final temperature were important determinants of the crystal structure and the final size of $CoFe_2O_4$-$BaTiO_3$ core shell MENs. For example, a temperature of 600 °C was required for 30-nm MENs.

B. Vibrating sample magnetometry

A cryogen-free 9-T vibrating sample magnetometer (VSM) physical property management system from Quantum Design was used to measure M-H loops and M-T dependence in a temperature ranging from 1.9 to 400 K.

C. Transmission electron microscopy (TEM)

A Phillips CM-200 200 kV Transmission Electron Microscope (TEM) with an Energy Dispersive Spectroscopy (EDS) option was used to obtain TEM images and EDS profiles.

D. Atomic force microscopy

The imaging of both glioblastoma and brain endothelia cells in a cellular microenvironment was conducted using a MultiMode AFM system. Using a Bruker electrochemistry fluid cell probe holder that has an integrated piezo element for contact mode experiments and Bruker's DNP-S10 silicon nitride probe, we were able to achieve the desired results showing the interaction between MENs and the surface of a cell. The DNP-S10 probe comes with four different cantilevers of various dimensions each having a different nominal spring constant value and resonant frequency. The special C triangular shape cantilever was used for cell imaging; the cantilever has a nominal resonant frequency of 56 kHz and a nominal spring constant of 0.24N/m which are ideal values for imaging stiff and firmly attached samples. After placing the probe in the liquid solution, which for this experiment was phosphate buffer solution (PBS), the resonant frequency dropped to 8 kHz, i.e., an order of magnitude lower compared to the frequency in air. After obtaining a lower resonant frequency, the probe was engaged with the membrane surface for scanning at a frequency rate of 0.100 Hz and a scan size of 100 nm; these two parameters were gradually increased until an adequate quality image was obtained.

[1] K. S. Chan, C. G. Koh, and H. Y. Li, Cell Death Dis. **3**, e411 (2012).
[2] J. K. Vasir and V. Labhasetwar, Technol. Cancer Res. Treat. **4**(4), 363–374 (2005).
[3] M. Yoshida, R. Takimoto, K. Murase, Y. Sato, M. Hirakawa, F. Tamura, T. Sato, S. Iyama, T. Osuga, K. Miyanishi, K. Takada, T. Hayashi, M. Kobune, and J. Kato, PLoS One **7**(7), e39545 (2012).
[4] E. M. Pridgen, R. Langer, and O. C. Farokhzad, Nanomedicine (London) **2**(5), 669–680 (2007).
[5] S. Shah, Y. Liu, W. Hu, and J. Gao, J. Nanosci. Nanotechnol. **11**(2), 919–928 (2011).
[6] D. Peer, J. M. Karp, S. Hong, O. C. Farokhzad, R. Margalit, and R. Langer, Nat. Nanotechnol. **2**(12), 751–760 (2007).
[7] A. Z. Wang, R. Langer, and O. C. Farokhzad, Annu. Rev. Med. **63**, 185–198 (2012).
[8] I. Brigger, C. Dubernet, and P. Couvreur, Adv. Drug Delivery Rev. **54**(5), 631–651 (2002).
[9] S. Barua, J. W. Yoo, P. Kolhar, A. Wakankar, Y. R. Gokarn, and S. Mitragotri, Proc. Natl. Acad. Sci. U. S. A. **110**(9), 3270–3275 (2013).
[10] R. Tong, H. D. Hemmati, R. Langer, and D. S. Kohane, J. Am. Chem. Soc. **134**(21), 8848–8855 (2012).
[11] U. Prabhakar, H. Maeda, R. K. Jain, E. M. Sevick-Muraca, W. Zamboni, O. C. Farokhzad, S. T. Barry, A. Gabizon, P. Grodzinski, and D. C. Blakey, Cancer Res. **73**(8), 2412–2417 (2013).
[12] H. Maeda, Adv. Enzyme Regul. **41**, 189–207 (2001).
[13] S. Kunjachan, R. Pola, F. Gremse, B. Theek, J. Ehling, D. Moeckel, B. Hermanns-Sachweh, M. Pechar, K. Ulbrich, W. E. Hennink, G. Storm, W. Lederle, F. Kiessling, and T. Lammers, Nano Lett. **14**(2), 972–981 (2014).
[14] F. Danhier, O. Feron, and V. Preat, J. Controlled Release **148**(2), 135–146 (2010).
[15] F. Brasseur, P. Couvreur, B. Kante, L. Deckers-Passau, M. Roland, C. Deckers, and P. Speiser, Eur. J. Cancer **16**(11), 1441–1445 (1980).
[16] I. Cheong, X. Huang, C. Bettegowda, L. A. Diaz, Jr., K. W. Kinzler, S. Zhou, and B. Vogelstein, Science **314**(5803), 1308–1311 (2006).
[17] D. W. Lee, D. M. Barrett, C. Mackall, R. Orentas, and S. A. Grupp, Clin. Cancer Res. **18**(10), 2780–2790 (2012).
[18] R. K. Oldham and R. O. Dillman, J. Clin. Oncol. **26**(11), 1774–1777 (2008).
[19] V. P. Torchilin, Nat. Rev. Drug Discovery **4**(2), 145–160 (2005).
[20] W. Tai, R. Mahato, and K. Cheng, J. Controlled Release **146**(3), 264–275 (2010).
[21] M. A. Firer and G. Gellerman, J. Hematol. Oncol. **5**, 70 (2012).
[22] X. Wei, X. Chen, M. Ying, and W. Lu, Acta Pharm. Sin. B **4**(3), 193–201 (2014).
[23] F. Danhier, E. Ansorena, J. M. Silva, R. Coco, A. Le Breton, and V. Preat, J Controlled Release **161**(2), 505–522 (2012).
[24] B. P. Timko, T. Dvir, and D. S. Kohane, Adv. Mater. **22**(44), 4925–4943 (2010).
[25] X. Li, Q. Zhao, and L. Qiu, J. Controlled Release **171**(2), 152–162 (2013).
[26] G. Wu, A. Mikhailovsky, H. A. Khant, C. Fu, W. Chiu, and J. A. Zasadzinski, J. Am. Chem. Soc. **130**(26), 8175–8177 (2008).
[27] W. Zhang, K. Gilstrap, L. Wu, K. C. Remant Bahadur, M. A. Moss, Q. Wang, X. Lu, and X. He, ACS Nano **4**(11), 6747–6759 (2010).

[28]M. C. Cochran, J. R. Eisenbrey, M. C. Soulen, S. M. Schultz, R. O. Ouma, S. B. White, E. E. Furth, and M. A. Wheatley, Acad. Radiol. **18**(11), 1341–1348 (2011).

[29]C. Y. Lin, J. R. Li, H. C. Tseng, M. F. Wu, and W. L. Lin, Nanomedicine **8**(6), 900–907 (2012).

[30]E. K. Lim, Y. M. Huh, J. Yang, K. Lee, J. S. Suh, and S. Haam, Adv. Mater. **23**(21), 2436–2442 (2011).

[31]D. Putnam and J. Kopecek, Bioconjugate Chem. **6**(4), 483–492 (1995).

[32]S. C. McBain, H. H. Yiu, and J. Dobson, Int. J. Nanomed. **3**(2), 169–180 (2008).

[33]S. L. McGill, C. L. Cuylear, N. L. Adolphi, M. Osinski, and H. D. Smyth, IEEE Trans. Nanobiosci. **8**(1), 33–42 (2009).

[34]B. Liu, X. Zhang, C. Li, F. He, Y. Chen, S. Huang, D. Jin, P. Yang, Z. Cheng, and J. Lin, Nanoscale **8**(25), 12560–12569 (2016).

[35]T. Hoare, J. Santamaria, G. F. Goya, S. Irusta, D. Lin, S. Lau, R. Padera, R. Langer, and D. S. Kohane, Nano Lett. **9**(10), 3651–3657 (2009).

[36]M. R. Prausnitz, V. G. Bose, R. Langer, and J. C. Weaver, Proc. Natl. Acad. Sci. U. S. A. **90**(22), 10504–10508 (1993).

[37]D. C. Chang, *Guide to Electroporation and Electrofusion* (Academic Press, San Diego, 1992).

[38]H. Y. Wang and C. Lu, Biotechnol. Bioeng. **95**(6), 1116–1125 (2006).

[39]C. Chen, S. W. Smye, M. P. Robinson, and J. A. Evans, Med. Biol. Eng. Comput. **44**(1–2), 5–14 (2006).

[40]H. Y. Wang and C. Lu, Biotechnol. Bioeng. **100**(3), 579–586 (2008).

[41]K. Cahill, Phys. Biol. **7**, 16001 (2009).

[42]V. Novickij, A. Grainys, E. Lastauskiene, R. Kananaviciute, D. Pamedytyte, L. Kalediene, J. Novickij, and D. Miklavcic, Sci. Rep. **6**, 33537 (2016).

[43]A. Silve, I. Leray, M. Leguebe, C. Poignard, and L. M. Mir, Bioelectrochemistry **106**(Pt B), 369–378 (2015).

[44]K. Redmann, V. Muller, S. Tanneberger, and W. Kalkoff, Acta Biol. Med. Ger. **28**(5), 853–856 (1972).

[45]S. Betal, B. Shrestha, M. Dutta, L. F. Cotica, E. Khachatryan, K. Nash, L. Tang, A. S. Bhalla, and R. Guo, Sci. Rep. **6**, 32019 (2016).

[46]K. Yue, R. Guduru, J. Hong, P. Liang, M. Nair, and S. Khizroev, PLoS One **7**(9), e44040 (2012).

[47]R. Guduru, P. Liang, C. Runowicz, M. Nair, V. Atluri, and S. Khizroev, Sci. Rep. **3**, 2953 (2013).

[48]R. Guduru, P. Liang, J. Hong, A. Rodzinski, A. Hadjikhani, J. Horstmyer, E. Levister, and S. Khizroev, Nanomedicine (London) **10**(13), 2051–2061 (2015).

[49]A. Rodzinski, R. Guduru, P. Liang, A. Hadjikhani, T. Stewart, E. Stimphil, C. Runowicz, R. Cote, N. Altman, R. Datar, and S. Khizroev, Sci. Rep. **6**, 20867 (2016).

[50]T. Lammers, F. Kiessling, W. E. Hennink, and G. Storm, J. Controlled Release **161**(2), 175–187 (2012).

[51]A. Kaushik, R. D. Jayant, R. Nikkhah-Moshaie, V. Bhardwaj, U. Roy, Z. Huang, A. Ruiz, A. Yndart, V. Atluri, N. El-Hage, K. Khalili, and M. Nair, Sci. Rep. **6**, 25309 (2016).

[52]W. Eerenstein, N. D. Mathur, and J. F. Scott, Nature **442**(7104), 759–765 (2006).

[53]S. Xie, F. Ma, Y. Liu, and J. Li, Nanoscale **3**(8), 3152–3158 (2011).

[54]S. Wang, W. Yang, H. Du, F. Guo, H. Wang, J. Chang, X. Gong, and B. Zhang, Nanotechnology **27**(16), 165101 (2016).

[55]N. Singh, G. J. Jenkins, R. Asadi, and S. H. Doak, Nano Rev. **1**, 5358 (2010).

[56]N. D. Thorat, O. M. Lemine, R. A. Bohara, K. Omri, L. El Mir, and S. A. Tofail, Phys. Chem. Chem. Phys. **18**(31), 21331–21339 (2016).

[57]T. Fu, Q. Kong, H. Sheng, and L. Gao, Neural Plast. **2016**, 2412958 (2016).

[58]M. Peng, H. Li, Z. Luo, J. Kong, Y. Wan, L. Zheng, Q. Zhang, H. Niu, A. Vermorken, W. Van de Ven, C. Chen, X. Zhang, F. Li, L. Guo, and Y. Cui, Nanoscale **7**(25), 11155–11162 (2015).

[59]T. Kimura, T. Goto, H. Shintani, K. Ishizaka, T. Arima, and Y. Tokura, Nature **426**(6962), 55–58 (2003).

[60]K. Ulbrich, K. Hola, V. Subr, A. Bakandritsos, J. Tucek, and R. Zboril, Chem. Rev. **116**(9), 5338–5431 (2016).

[61]L. C. Barnsley, D. Carugo, M. Aron, and E. Stride, Phys. Med. Biol. **62**, 2333 (2017).

[62]N. V. Long, Y. Yang, T. Teranishi, C. M. Thi, Y. Cao, and M. Nogami, J. Nanosci. Nanotechnol. **15**(12), 10091–10107 (2015).

[63]A. Busato, R. Bonafede, P. Bontempi, I. Scambi, L. Schiaffino, D. Benati, M. Malatesta, A. Sbarbati, P. Marzola, and R. Mariotti, Int. J. Nanomed. **11**, 2481–2490 (2016).

[64]J. Weizenecker, B. Gleich, J. Rahmer, H. Dahnke, and J. Borgert, Phys. Med. Biol. **54**(5), L1–L10 (2009).

[65]M. Nair, R. Guduru, P. Liang, J. Hong, V. Sagar, and S. Khizroev, Nat. Commun. **4**, 1707 (2013).

[66]R. Binggeli and I. L. Cameron, Cancer Res. **40**(6), 1830–1835 (1980).

[67]S. J. Beebe, N. M. Sain, and W. Ren, Cells **2**(1), 136–162 (2013).

[68]V. Corral-Flores, D. Bueno-Baqués, and R. Ziolo, Acta Mater. **58**, 764 (2010).

[69]C. Schmitz-Antoniak, D. Schmitz, P. Borisov, F. M. de Groot, S. Stienen, A. Warland, B. Krumme, R. Feyerherm, E. Dudzik, W. Kleemann, and H. Wende, Nat. Commun. **4**, 2051 (2013).

[70]M. Scigaj, N. Dix, J. Gazquez, M. Varela, I. Fina, N. Domingo, G. Herranz, V. Skumryev, J. Fontcuberta, and F. Sanchez, Sci. Rep. **6**, 31870 (2016).

[71]H. Zheng, J. Wang, S. E. Lofland, Z. Ma, L. Mohaddes-Ardabili, T. Zhao, L. Salamanca-Riba, S. R. Shinde, S. B. Ogale, F. Bai, D. Viehland, Y. Jia, D. G. Schlom, M. Wuttig, A. Roytburd, and R. Ramesh, Science **303**(5658), 661–663 (2004).

[72]B. R. Pieters, D. Z. D. Back, C. C. Koning, and A. H. Zwinderman, Radiother. Oncol. **93**, 168 (2009).

[73]J. Hong, E. Bekyarova, P. Liang, W. A. D. Heer, R. C. Haddon, and S. Khizroev, Sci. Rep. **2**, 624 (2012).

[74]I. Weinberg, "MRI-guided nanoparticle cancer therapy apparatus and methodology," U.S. patent 2013/0046169 A1 (2013).

[75]H. Nakamura, F. Jun, and H. Maeda, Expert Opin. Drug Delivery **12**, 53 (2014).

[76]C. C. Roth, G. P. Tolstykh, J. A. Payne, M. A. Kuipers, G. L. Thompson, M. N. Desilva, and B. L. Ibey, J. Biomed. Opt. **18**, 035005 (2013).

[77]F. M. Veronese and G. Pasut, Drug Discovery Today **10**, 1451 (2005).

[78]G. Pillai, SOJ Pharm. Pharm. Sci. **1**, 1 (2014).